npj Systems Biology and Applications https://doi.org/10.1038/s41540-026-00662-x

Article in Press

Ecological and stochastic determinants of the growth and persistence of the oral pathogen *Porphyromonas gingivalis*

Received: 9 November 2025

Accepted: 31 January 2026

Cite this article as: Hussein, M., Barua, A., Qasaimeh, M. *et al.* Ecological and stochastic determinants of the growth and persistence of the oral pathogen *Porphyromonas gingivalis*. *npj Syst Biol Appl* (2026). https://doi.org/10.1038/s41540-026-00662-x

Moemen Hussein, Arnab Barua, Mohammad Qasaimeh, Matthew Smardz, Patricia I. Diaz & Haralampos Hatzikirou

Ecological and Stochastic Determinants of the Growth and Persistence of the Oral Pathogen Porphyromonas gingivalis

Moemen Hussein[1,2†], Arnab Barua[3,4†], Mohammad Qasaimeh[7,8,9,10], Matthew Smardz[5,6], Patricia I. Diaz[5,6], Haralampos Hatzikirou[3,4*]

[1]Department of Biomedical Engineering and Biotechnology, Khalifa University, Abu Dhabi, UAE.
[2]Department of Mathematical Engineering and Physics, Faculty of Engineering, Alexandria University, Alexandria, Egypt.
[3]Mathematics Department, Khalifa University, Abu Dhabi, UAE.
[4]Center for Information Services and High Performance Computing, Technische Universität Dresden, Dresden, Germany.
[5]UB Microbiome Center, University at Buffalo, Buffalo, NY, USA.
[6]Department of Oral Biology, School of Dental Medicine, University at Buffalo, Buffalo, NY, USA.
[7]Division of Engineering, New York University Abu Dhabi, Abu Dhabi, UAE.
[8]Department of Mechanical and Aerospace Engineering, New York University, Brooklyn, NY, USA.
[9]Department of Biomedical Engineering, New York University, Brooklyn, NY, USA.
[10]Research Center for Translational Medical Devices, New York University Abu Dhabi, Abu Dhabi, UAE.

*Corresponding author(s). E-mail(s): haralampos.hatzikirou@ku.ac.ae;
†These authors contributed equally to this work.

Abstract

Population density plays a critical role in microbial fitness. However, its influence on pathogen colonization remains incompletely understood. *Porphyromonas*

gingivalis (Pg) is a pathogen that plays a major role in periodontitis. It exhibits Allee-type growth and requires a quorum threshold to replicate. Yet, it is frequently detected at low abundance *in vivo*. We integrate quantitative growth experiments with mathematical modeling to identify ecological and stochastic determinants of Pg persistence. A cubic Allee-effect model quantifies a quorum threshold below which populations collapse. Conditioned medium from *Veillonella parvula* (Vp) lowers this threshold, indicating early-colonizer facilitation. Stochastic extensions and Fokker–Planck analysis show that microenvironmental noise enables persistence below the Allee barrier. This behavior is consistent with long-term subthreshold experiments that yield persistent survival. Pg–Vp co-cultures further demonstrate replicate rescue outcomes for subcritical inocula. Vp reliably reaches capacity, constraining terminal phases within the experimental horizon to coexistence or Pg extinction. A two-species replicator model maps these outcomes onto a (β, γ) plane. This mapping restricts accessible regions once Vp is established and suggests interventions that reduce facilitation and limit Pg-associated inflammation.

Keywords: Porphyromonas gingivalis, Periodontitis, Allee effect, Microbial heterogeneity, Noise-induced phase transitions, Evolutionary game-theory

Introduction

Periodontitis is among the most prevalent chronic inflammatory diseases, affecting nearly half of the global adult population [1]. Beyond local tissue destruction and tooth loss, periodontitis is now recognized as a systemic disease modifier that contributes to cardiovascular disorders, metabolic dysregulation, adverse pregnancy outcomes, and neurodegenerative conditions [2–4]. Despite this broad health burden, the microecological and biophysical principles that allow periodontal pathogens to persist and destabilize microbial communities remain incompletely understood [5, 6].

As a multifactorial, biofilm-driven condition, periodontitis emerges through a shift in the oral microbiota from a commensal-dominated, health-associated state (eubiosis) to a pathogen-enriched, pro-inflammatory configuration (dysbiosis) [6, 7]. These contrasting states can be understood as alternative stable equilibria of the microbial community. Eubiosis reflects a balanced composition that resists pathogen overgrowth and supports immune homeostasis, whereas dysbiosis is characterized by the enrichment of *Porphyromonas gingivalis* (Pg) and other pathogens, promoting sustained inflammation and tissue destruction [8].

Central to this transition is Pg, a Gram-negative obligate anaerobe that, even at low relative abundance, can remodel microbial community structure and modulate host immune surveillance [9, 10]. This observation, formalized in the keystone pathogen hypothesis, reframes pathogenicity in terms of ecological impact rather than absolute population dominance [11]. However, most studies have focused on individual virulence factors or host interactions in isolation, rather than examining how ecological thresholds, stochastic survival strategies, and cross-species interactions combine to determine Pg persistence [12–14].

A paradox emerges from this perspective, as Pg is frequently detected at low levels in both healthy and diseased conditions despite exhibiting Allee-type growth behavior [10, 15], a form of inverse density dependence in which population growth becomes negative below a critical threshold [16]. Classical population theory would therefore predict extinction of subthreshold populations, yet clinical studies report that Pg may persist, if at low abundance, in a fraction of individuals with periodontal health [17, 18] or reappear after antimicrobial or mechanical debridement [19–21]. This discrepancy implies that buffering mechanisms enable Pg to cross or bypass deterministic extinction thresholds and push the community toward the dysbiotic basin of attraction [14, 22].

One such mechanism may be microbial facilitation. In polymicrobial communities, metabolic interdependence and cooperative interactions are common [6, 14]. *Veillonella parvula* (Vp), an early colonizer of oral biofilms, co-occupies niches with Pg and may supply diffusible growth factors or alter redox conditions to favor Pg establishment [6, 15, 23]. *In vitro* studies support this hypothesis, showing that Vp-conditioned medium can significantly alter Pg growth dynamics and lower its effective colonization threshold [12, 15]. However, the magnitude and mechanism of this facilitation remain to be fully elucidated [23].

In addition to facilitation, stochastic effects stemming from microenvironmental variability may enable Pg populations to survive at densities where deterministic models predict extinction [9, 15, 24, 25]. Phenotypic heterogeneity, arising from gene-expression noise and micro-niche variation, has been shown to confer survival advantages through bet-hedging strategies [2, 14, 26]. For Pg, such heterogeneity could represent a crucial colonization tactic, helping push populations across the tipping point that separates extinction from dominance [26].

Lastly, the dynamics of colonization are shaped by nonlinear, frequency-dependent interspecies interactions. Evolutionary game theory offers a principled framework for describing how competition and cooperation generate alternative stable states in microbial communities [27, 28]. In the Pg–Vp system, cooperation may underlie dysbiotic transitions, whereas competition may correspond to eubiotic resilience where Pg fails to replicate [6].

In this study, we integrate quantitative experiments with mathematical modeling to address three questions: (i) How does Vp influence the colonization threshold of Pg? (ii) Can heterogeneity-driven noise promote Pg persistence below deterministic thresholds? (iii) Can we identify the Pg-Vp interactions that lead to experimentally observed dynamic phases (microbiome constellations)? To answer these, we parameterize an Allee-effect model, quantify Vp-driven threshold shifts, incorporate stochasticity to explore noise-induced rescue, and use a replicator equation along with new Pg-Vp coculture experiments to map potential bacterial interactions in their corresponding phases.

Together, these approaches establish a systems-level perspective on Pg microecology and provide a quantitative basis for explaining the persistence of this pathogen despite its strong Allee dependency. Understanding these ecological mechanisms is essential for designing targeted interventions that prevent Pg colonization or

restore microbial homeostasis to mitigate the systemic consequences of chronic oral inflammation [6, 11].

Results

Critical Pg Density Threshold: Experimental Evidence for Allee Effect

A central question in oral microbial ecology is why *Porphyromonas gingivalis* (Pg) can persist at low levels in some individuals but becomes extinct in others. To address this, we modelled Pg population growth using a cubic Allee-effect differential equation, which encapsulates the principle that populations must surpass a critical quorum to sustain growth [29]. The model equation reads:

$$\frac{dN}{dt} = rN\left(1 - \frac{N}{K}\right)\left(\frac{N}{A} - 1\right) \tag{1}$$

Here, $N(t)$ is the Pg population (gene copies/ml) at time t, r is the intrinsic growth rate, K is the carrying capacity, and A is the Allee threshold. The last term encodes inverse density dependence, when $N < A$ growth becomes negative and the population heads toward extinction.

This model was fitted to experimental time-series data [15] using a global differential evolution-based optimization [30], in which the parameters r, K, and A were estimated simultaneously across all experimental concentrations by minimizing the aggregate error between observed and predicted $\log_{10}$-transformed population sizes. Fitting this model to the experimental growth curves yielded $r = 0.6529 \pm 7.1 \times 10^{-6}$, $K = 2.08 \times 10^9 \pm 2.02 \times 10^5$, and $A = 4.59 \times 10^7 \pm 2.6 \times 10^3$, closely reproducing the experimental observations (see Figure 1). The small uncertainty in r reflects its strong identifiability from the early growth phase, while K and A are constrained by saturation and survival-extinction dynamics. Further details for the parameter estimation process can be found in Supplementary Note 2.

Please note that the Pg decline after reaching the theoretical capacity can be mediated by nutrient depletion or metabolic waste buildup [31], phenomena that are not captured by our rudimentary model. These results provide quantitative evidence that Pg requires a minimal quorum to escape extinction.

This threshold shows why Pg is rarely sustained in healthy oral microbiomes. Host immune clearance and competitive commensals keep Pg below the A threshold. Once the threshold is crossed, however, Pg growth becomes self-reinforcing, establishing a dysbiotic community that is difficult to reverse.

Vp-Derived Metabolites Facilitate Pg Persistence at Subcritical Densities

Because the estimated Allee threshold A is high relative to Pg abundances in periodontal health and even moderate periodontitis, we asked to what extent facilitation by early colonizers lowers this barrier. We therefore quantified the effect of diffusible Vp metabolites on the effective threshold by growing Pg in media supplemented with

cell-free Vp-conditioned supernatant harvested after 24 h and re-estimating A under these conditions [15].

The Allee model was re-fitted to the Pg-Vp spent medium data

$$\frac{dN}{dt} = rN\left(1 - \frac{N}{K}\right)\left(\frac{N}{A_{Vp}} - 1\right), \tag{2}$$

where A_{Vp} is the metabolite-modified threshold. The fitted results showed a significant reduction in A_{Vp} compared to previously estimated A across all tested spent medium concentrations (Figure 2b). This suggests that Vp-derived metabolites lower the minimum population size required for Pg persistence.

Vp-conditioned medium lowered the fitted Allee threshold relative to baseline ($A_{Vp} < A$), but the effect was condition-dependent. For example, as shown in Figure 2a, at 25% Vp SM, subcritical Pg inocula failed to grow, consistent with the fitted $A_{Vp} = 1.1 \times 10^6 \pm 4.09 \times 10^1$ remaining above the starting density of 1.09×10^6 (Figures 2a, 2b). Across SM levels, estimates of r and K also varied (Figure 2b), but the key factor for Pg growth persistence was the shift in A, which defines the extinction–persistence boundary. These parameter variabilities, together with the recurrent detection of low-abundance Pg *in vivo*, motivate a stochastic extension in which A and r stochastically fluctuate to model microenvironmental and demographic noise.

Microenvironmental Noise Enables Pg Persistence

The deterministic Allee model captures how Vp-derived metabolites lower the Pg persistence threshold, but it cannot explain replicate-to-replicate variability near this barrier. *In vivo*, bacterial populations are exposed to complex fluctuations affecting both their inherent proliferation ability (demographic noise in the sense of nutrient fluctuations) and their quorum sensing thresholds (environmental noise in the sense of diffusion rates or signal interference). Such fluctuations can intermittently support persistence below the deterministic Allee threshold.

The impact of proliferation and Allee threshold noise correlation

To capture this variability, we generalize the model by introducing distinct stochastic fluctuations for the proliferation rate (r) and the Allee threshold (A):

$$A(t) = A_m(1 + \eta_A(t)), \tag{3}$$

$$r(t) = r_m(1 + \eta_r(t)), \tag{4}$$

where η_A and η_r are Gaussian white noises with intensities σ_A, σ_r and a correlation coefficient $\lambda \in [-1, 1]$. This formulation acknowledges that environmental cues often impact multiple biological parameters simultaneously.

Substituting these stochastic terms into the general population equation yields the following Stochastic Differential Equation (SDE):

$$\frac{dN}{dt} = \frac{r_m(1 + \eta_r(t))}{A_m(1 + \eta_A(t))} N\left(1 - \frac{N}{K}\right)\left(N - A_m(1 + \eta_A(t))\right). \tag{5}$$

Assuming small noise amplitudes ($\sigma_r, \sigma_A \ll 1$), we linearize the pre-factor term as $(1+\eta_r)(1+\eta_A)^{-1} \approx 1+\eta_r-\eta_A$. The noise is interpreted as $\eta(t) = \frac{dW_t}{dt}$ in the distributional sense, where W_t denotes a Wiener process. Expanding the terms and keeping contributions up to the first order in noise, we obtain a Langevin equation driven by two correlated noise sources:

$$\frac{dN}{dt} \approx f(N) + f(N)\underbrace{(\eta_r(t) - \eta_A(t))}_{\eta_{eff}} \underbrace{-r_m N\left(1-\frac{N}{K}\right)}_{g_A(N)}\eta_A(t), \tag{6}$$

where $f(N)$ is the deterministic rate and $g_A(N)$ describes how threshold fluctuations couple to the population state.

Applying an extended mean-field analysis to this multi-noise system (see Supplementary Note 1 for the detailed derivation via Novikov's theorem), we determined the sensitivity of the critical saddle node (N^*) to these coupled fluctuations. Our analysis reveals that the correlation λ acts as a control parameter for population stability, with the saddle node shift obeying:

$$\delta N^* = r_m A_m \left[\lambda\sigma_r\sigma_A\left(1-\frac{A_m}{K}\right) - \sigma_A^2\left(2-\frac{3A_m}{K}\right)\right]. \tag{7}$$

Assuming that $A_m \ll K$, this implies a biological dichotomy:

- **Positive Correlation ($\lambda > 0$):** If growth-rate and Allee-threshold fluctuations are positively correlated, the saddle node shifts to higher densities. For example, high fluid flow rates increase nutrient supply but also wash away autoinducers and secreted enzymes. This process demands higher bacterial densities to maintain quorum [32]. As a result, the extinction basin expands, and the Pg population becomes more vulnerable.
- **Negative Correlation ($\lambda < 0$):** A negative correlation produces a "buffering" effect. In nutrient-rich environments, the need for cooperative resource acquisition often decreases [33]. This shift moves the saddle node toward zero. Survival becomes more likely even at lower densities.
- **Zero correlation ($\lambda = 0$):** For statistically independent noises, the quantity δN^* is always negative. This outcome enhances Pg survival by lowering the effective threshold. It is likely the most common scenario, since proliferation and quorum sensing operate on different time scales.

Environmental effective noise and experimental comparisons

While the two-noise framework provides a theoretical basis for how correlation shapes stability, experimentally distinguishing η_r from η_A requires high-resolution single-cell time traces. Therefore, to parameterize the net effect of these fluctuations against our longitudinal population data, we utilize an *effective single-noise approximation*. We lump the correlated sources into a single effective noise term $\eta(t)$ with intensity ϵ. Moreover, this assumption imposes no conditions on the noise magnitude.

To reflect this variability, we incorporated environmental and demographic noise into the model by allowing the threshold (A) and proliferation rate (r) to fluctuate. These stochastic terms collectively account for variability in microenvironmental conditions and cell-to-cell heterogeneity affecting proliferation and sensing behavior.

$$A(t) = A_m(1 + \sqrt{\epsilon}\eta(t)) \tag{8}$$
$$r(t) = r_m(1 + \sqrt{\epsilon}\eta(t)), \tag{9}$$

where $\eta(t)$ is Gaussian white noise, with $\langle \eta(t) \rangle = 0$ and $\langle \eta(t)\eta(t') \rangle = \delta(t - t')$, and ϵ controls the overall noise intensity. Using the assumption $\eta(t) = \eta_A(t) = \eta_r(t)$ and substituting in Eq. (6), we obtain:

$$\frac{dN}{dt} = \tilde{r}N\left(1 - \frac{N}{K}\right)\left(N - A_m(1 + \sqrt{\epsilon}\eta(t))\right), \tag{10}$$

where $\tilde{r} = r_m/A_m$ is a rescaled proliferation rate. We interpret the above equation in the Itô sense; $N = 0$ (extinction) and $N = K$ (capacity) are natural/absorbing boundaries unless stated otherwise. This results in the stochastic differential equation:

$$dN = f(N)\, dt + \sqrt{\varepsilon}\, g(N)\, dW_t, \tag{11}$$

where W_t denotes a Wiener process, and $\eta(t) = \frac{dW_t}{dt}$ is understood in the distributional sense, with

$$f(N) = \tilde{r}N\left(1 - \frac{N}{K}\right)(N - A_m),$$
$$g(N) = -r_m N\left(1 - \frac{N}{K}\right)$$

Assuming small noise intensity $\epsilon \ll 1$, we can apply Novikov's theorem [34, 35] to obtain an extended mean-field approximation:

$$\frac{dN}{dt} = f(N) + \epsilon_0 \frac{dg(N)}{dN} g(N) \tag{12}$$

The term $\epsilon_0\, g'(N)g(N)$ represents the mean-field correction for multiplicative noise. Since we interpret Eq. (11) in the Itô sense, we treat ϵ_0 as an effective fitted coefficient. After some algebra, the mean-field equation reads:

$$\frac{dN}{dt} = N(1 - \frac{N}{K})\Big[\tilde{r}(N - A_m) + \epsilon_0 r_m^2(1 - 2\frac{N}{K})\Big]. \tag{13}$$

As one observes, the third term on the right-hand side allows us to calculate the new saddle node, which depends on the noise intensity:

$$N^* = \frac{\tilde{r}A_m - \varepsilon_0 r_m^2}{\tilde{r} - \frac{2\varepsilon_0 r_m^2}{K}} \approx A_m - \epsilon_0 r_m A_m, \tag{14}$$

since the term $\frac{2\varepsilon_0 r_m^2}{K} \ll 1$. Therefore, noise shifts the saddle node, i.e., Allee threshold, towards zero (see Figure 3). Thus, minimal quorum-sensing noise lowers the effective Allee barrier by $\approx \epsilon_0 r_m A_m$, increasing the chance of under-threshold rescue. This approximation is valid only for small noises, as a prerequisite for Novikov's theorem.

At higher noise amplitudes ($\epsilon \gg 1$), populations initiated above the Allee threshold ($N_0 > A$) remained robust to stochastic fluctuations and maintained populations near carrying capacity (Figure 4a). In contrast, when populations started below the threshold ($N_0 < A$), stochastic variability occasionally enhanced survival by sustaining persistence at low abundances, thereby rescuing populations from extinction (Figure 4b).

To validate the predictions of the stochastic model, we first conducted long-term experimental observations of subthreshold Pg cultures. We then derived the corresponding steady-state probability distribution using the Fokker–Planck equation and compared it with the long-term subthreshold laboratory cultures of Pg.

Figure 5 shows the experimentally measured Pg trajectories over time and the corresponding steady-state distribution, based on observations up to 32 days across 27 biological replicates. The data reveal heterogeneous outcomes. Some populations collapsing to very low abundances ($N \lesssim 10^2$) at different rates, while others maintain higher population levels ($N \gtrsim 10^5$) after fluctuating around the threshold.

This diversity of outcomes is consistent with the stochastic model predictions, where random fluctuations can drive populations either toward extinction or persistence. The limited number of observations at intermediate abundances ($10^2 < N < 10^5$) suggests that populations spending relatively little time in this unstable region. As shown in Figure 5a, individual trajectories exhibit such noise-driven fluctuations near the Allee threshold before stabilizing at low or high abundance levels. Together, these results demonstrate strong agreement between the experimental observations and the stochastic model, supporting the interpretation that Pg population dynamics are governed by stochastic transitions between extinction and persistence within a metastable landscape.

For a quantitative link between stochastic dynamics and population persistence, we computed the temporal evolution and steady-state probability distribution of the Pg population from the corresponding Fokker–Planck equation (FPE) derived from Eq. (11).

$$\frac{\partial p(N,t)}{\partial t} = -\frac{\partial}{\partial N}(f(N)p(N,t)) + \frac{\epsilon}{2}\frac{\partial^2}{\partial N^2}(g^2(N)p(N,t)) \tag{15}$$

The equilibrium distribution for the multiplicative noise FPE reads:

$$p_{eq}(N) = \frac{C}{g^2(N)} \exp\left(\int^N \frac{2\, f(u)}{\epsilon g^2(u)}\, du \right).$$

Please note that the FPE does not require any assumption for the noise amplitude ϵ. The resulting stationary probability density $p_{eq}(N)$ captures the expected bimodality of the experimentally measured frequency distribution, as calculated from 27

independent replicates initiated below the deterministic Allee threshold.

$$p_{eq}(N) = C\frac{K^2}{r_m^2}N^{-2-\frac{2}{\epsilon r_m}}(K-N)^{-2-2\left(\frac{K-A_m}{\epsilon r_m A_m}\right)}, \qquad 0 \le N \le K. \tag{16}$$

The steady-state distribution $p_{eq}(N)$ resembles a Beta-like distribution with compact support between $[0, K]$, consistent with the bounded nature of bacterial population sizes. For our Pg growth experiments, a truncated power law trend $p_{eq}(N) \propto N^{-\alpha}$ was observed near the extinction state with an estimated exponent of $\alpha = 2.47 \pm 0.60$ (95% CI: [1.81, 5.52]). Plugging into our theoretical exponent $\alpha = 2 + \frac{2}{\epsilon\, r_m}$ the experimentally obtained value, we find that the $\epsilon \ge 2.86$. Unfortunately, fitting the full distribution is difficult since we do not have observations close to the capacity. Moreover, the high-N part of the distribution depends on the A_m, K parameters, whose baseline values were fitted using 16SrRNA gene experiments (see Figure 1). Therefore, we cannot fit the full distribution since these baseline values overestimate the ones that correspond to CFU densities of Figure 5a [36]. This measurement discrepancy is not influencing the estimation of the proliferation rata r_m [37]. The fitted ϵ reflects the minimal intrinsic noise level that enables under-threshold populations to persist (see Figure 5b). Biologically, the inferred ε quantifies a minimal microenvironmental-sensing noise sufficient to rescue underthreshold inocula; *in vivo*, additional host and community variability will further increase effective noise, raising the probability of escapes across the Allee barrier.

In summary, incorporating noise into the Allee framework reveals that random fluctuations can shift the effective persistence threshold and rescue populations that would otherwise collapse. This stochastic mechanism provides a quantitative explanation for the intermittent detection of Pg at low abundance *in vivo* and indicates that persistence is not purely deterministic. Instead, phenotypic heterogeneity and micro-niche variability likely act as bet-hedging strategies that promote long-term survival.

Microecological Phase Transitions Driven by Pg–Vp Interactions

To investigate how pairwise interactions shape microecological dynamics, we focused on a system comprising Pg and Vp. This approach allows us to explore fundamental ecological behaviors that may underlie more complex community transitions.

For mechanistic modeling purposes, we describe the possible outcomes of the Pg–Vp system using four terms: **Pg extinction**, **Pg dominance**, **stable coexistence**, and **bistability**. These terms capture the distinct dynamical states predicted by our model and reflect alternative ecological attractors that can emerge from pairwise interactions.

Let N_{Pg} and N_{Vp} denote the absolute abundances of Pg and Vp, respectively, and $N_{total} = N_{\mathrm{Pg}} + N_{\mathrm{Vp}}$ the total number of bacteria. We define the normalized relative abundance of Pg as:

$$x = \frac{N_{\mathrm{Pg}}}{N_{total}}, \qquad 1 - x = \frac{N_{\mathrm{Vp}}}{N_{total}},$$

so that $x \in [0, 1]$ fully characterizes the community composition. The four qualitatively distinct outcomes can then be described as follows:

- **Pg extinction:** Pg is either absent or remains at low relative frequency, and the community resists Pg invasion ($x = 0$ is a stable equilibrium).
- **Pg dominance:** Pg proliferates and becomes dominant, leading to a Pg-dominated community ($x = 1$ or a Pg-dominated interior equilibrium is stable).
- **Stable coexistence:** An interior equilibrium $0 < x^\star < 1$ exists and is stable, indicating that Pg and Vp persist together at steady state.
- **Bistability:** Both $x = 0$ (Pg extinction) and $x = 1$ (Pg dominance) are stable equilibria, separated by an unstable interior threshold $x^\star$. The final outcome depends on initial conditions, reflecting historical contingency in community assembly.

Each species' fitness is determined by its interactions with Pg and Vp, encoded in the payoff matrix

$$\mathbf{A} = \begin{pmatrix} a_{11} & a_{12} \\ a_{21} & a_{22} \end{pmatrix},$$

where a_{ij} is the payoff to species i when interacting with j. The expected fitnesses are

$$f_{\mathrm{Pg}}(x) = a_{11}x + a_{12}(1 - x), \qquad f_{\mathrm{Vp}}(x) = a_{21}x + a_{22}(1 - x).$$

The replicator equation is the dynamical core of evolutionary game theory that translates payoff matrices into population dynamics [38, 39]. Here, the replicator equation states that the rate of change of x is proportional to Pg's excess fitness over the population mean:

$$\frac{dx}{dt} = x\big(f_{\mathrm{Pg}}(x) - \bar{f}(x)\big), \qquad \bar{f}(x) = x f_{\mathrm{Pg}}(x) + (1 - x) f_{\mathrm{Vp}}(x).$$

For two species, this simplifies to

$$\frac{dx}{dt} = x(1 - x)\big(f_{\mathrm{Pg}}(x) - f_{\mathrm{Vp}}(x)\big). \tag{17}$$

Substituting the linear fitness functions gives:

$$f_{\mathrm{Pg}} - f_{\mathrm{Vp}} = \underbrace{(a_{12} - a_{22})}_{\beta} + \underbrace{(a_{11} - a_{12} - a_{21} + a_{22})}_{\gamma} x,$$

and hence the normalized Eq. (17) reduces to a single cubic ODE:

$$\frac{dx}{dt} = x(1 - x)(\beta + \gamma x) = \gamma x(1 - x)(x + \frac{\beta}{\gamma}). \tag{18}$$

The parameter β quantifies Pg's relative advantage when interacting with Vp (against Vp with itself) and γ compares self-interaction against cross-species fitness changes. The system has three equilibria: ($x = 0$) (Pg extinction), ($x = 1$) (Pg dominance), and ($x^\star = -\beta/\gamma$) (an interior tipping point if ($0 < x^\star < 1$)). Stability analysis

shows that ($x = 0$) is stable when ($\beta < 0$), ($x = 1$) is stable when ($\beta + \gamma > 0$), and ($x^\star$) is an unstable saddle if ($\gamma > 0$). On the other hand, the ($x^\star$) can become stable when $\beta < 0$ and $\beta + \gamma > 0$. Table 1 resumes the biological interpretation of our stability analysis results. Using the stability conditions of γ and β parameters for the replicator Eq. (18), one can compute a phase space diagram as shown in Figure 6 where four phases/attractors lie (Extinction, Dominance, Coexistence, and Bistability state), separated by two boundaries (i.e., $\beta + \gamma = 0$ and $\beta = 0$).

To constrain our theoretical results, we performed Pg-Vp co-culture experiments under a subcritical inoculum ($N(0) = 10^5$). When Vp was co-cultured with Pg on Day 0, all replicates exhibited sustained growth, reaching near carrying capacity levels, consistent with strong early cross-species facilitation (Figure 7a). In contrast, when Vp was introduced only after the onset of population decline (Day 9), the outcomes varied. In several replicates, Pg regained growth to high densities following several days of sustained population levels ('Expansion'), whereas in others, the population was stochastically rescued ("Rescue") or sometimes went extinct despite Vp addition. Notably, when Pg was cultured alone before adding Vp, decline occurred in all replicates but at variable rates, consistent with the stochastic model predictions of noise-driven variability in time to extinction (Figure 4b).

By the end of all co-culture assays, Vp consistently reaches (or closely approaches) its carrying capacity (own experimental data). Although Vp time series are not available, imposing restrictions on the identifiability of the payoff matrix, this terminal saturation imposes a strong phase constraint: Pg-dominant endpoints are not observed. Within the experimental horizon, attainable terminal states reduce to two possibilities: (i) *coexistence*, with Pg at positive abundance while Vp occupies (near-)capacity; or (ii) *Pg extinction*, with Vp alone persisting. Stochasticity blurs the separatrix between these outcomes, producing the observed replicate variability. This experimental constraint on our phase space events has interesting implications for Pg-Vp interaction payoff parameters. Our experiments suggest $\beta + \gamma < 0 \implies \alpha_{11} < \alpha_{21}$. Assuming that subcritical inoculation of Pg implies $\alpha_{11} < 0$, no Pg-on-Vp interaction needs to be assumed. If the Vp facilitation on Pg is larger than the contribution of Vp self-renewal, i.e. $\beta > 0 \implies \alpha_{12} > \alpha_{22}$, it leads to bacterial coexistence. The latter can explain the Pg rescue in the presence of Vp (even when added at later times), since the Pg elimination state $x = 0$ becomes unstable. Figure 7b schematically recapitulates our findings.

Discussion

Dysbiosis in periodontitis is increasingly recognized as a microecological phase transition in the oral microbiome, in which a polymicrobial community enriched with pathobionts such as Porphyromonas gingivalis emerges and disrupts the balanced commensal community [9, 40]. Our results unify experimental observations and theory by demonstrating that Pg persistence emerges from the interplay of (i) density-dependent growth with an Allee threshold, (ii) cross-species facilitation by Vp, and

(iii) stochastic fluctuations possibly induced by environmental and phenotypic heterogeneity. Together, these mechanisms explain how Pg can persist at low densities *in vivo* despite deterministic predictions of extinction (see Figure 8).

Our deterministic Allee model quantitatively confirms the existence of a critical density threshold (A) below which Pg populations collapse, consistent with microenvironmental-sensing theory and the cooperative traits required for virulence and biofilm maturation [16, 41]. Importantly, the addition of Vp-conditioned medium lowered this threshold, supporting the idea that Vp functions as an ecological enabler that metabolically primes the niche for Pg colonization [15, 24]. While the metabolic cues required for Pg to support its own growth or those provided by Vp to Pg have not been identified yet, our work supports earlier findings which suggested Veillonella has a central role in the establishment of multi-species dental plaque communities [25, 31, 42]. Veillonella are prevalent dental plaque colonizers, previously recognized as a "core" subgingival species, which are proposed as generalists that play a central metabolic role supporting eubiosis to dysbiosis microbiome shifts

Incorporating stochasticity revealed that noise can rescue subcritical populations [43–45]. This result reframes Pg detection at low levels as a natural outcome of noise-driven survival and bet-hedging strategies [14, 46]. Additionally, by analyzing the corresponding FPE equilibrium distribution, we could obtain a quantitative noise estimate that is in line with the observed frequencies of sub-threshold survival. Clinical and experimental evidence supports this view: Few Pg cells can survive intracellularly [47, 48] and form persister subpopulations that tolerate antibiotics and re-initiate growth when stress abates [49–51]. Although our model does not explicitly resolve single-cell behavior, we hypothesize that fluctuations in cue thresholds, signal concentrations, or cellular responsiveness could generate phenotypic variability. Such heterogeneity may increase the likelihood of persistence at low densities, linking molecular variation to population outcomes.

Finally, our exploratory game-theoretic model captures the context-dependent switch between competitive and cooperative regimes. Mapping Pg–Vp dynamics in the (β, γ)-plane shows that Pg extinction corresponds to a globally attracting $x = 0$ state when $\beta < 0$, whereas Pg replication dominates when $\beta + \gamma > 0$. The bistable regime highlights the potential for history-dependent outcomes: once the community is perturbed across the tipping point $x^\star = -\beta/\gamma$, it will commit to Pg-dominance, even if the parameters remain unchanged. This provides a quantitative framework for understanding why Pg colonization can be difficult to reverse once established. In co-culture, subcritical Pg inocula exhibited replicate-to-replicate variable outcomes, as expected for noise-assisted persistence in a facilitated background. Notably, Vp reliably saturated to near carrying capacity by the end of the experiment; as a result, Pg-dominant endpoints were not observed, and the attainable terminal phases within the experimental horizon were reduced to two: *coexistence* (Pg persists with Vp at capacity) or *Pg extinction*. The coexistence phase can be interpreted as a proxy for the oral dysbiosis state. In our experiments, we mainly observe Pg-Vp coexistence, since even when Pg is at very low abundance, Vp introduction can still destabilize the zero Pg state.

Translationally, these findings suggest that therapeutic strategies should focus on shifting β to negative values, thereby restoring eubiosis as the global attractor. Potential approaches include (i) promoting competitive colonizers to reduce Pg fitness (a_{12}), (ii) disrupting metabolic facilitation pathways provided by Vp, (iii) enhancing host immune clearance of Pg, and (iv) timed ecological reseeding following biofilm disruption. These strategies can be systematically tested by monitoring longitudinal Pg trajectories and inferring effective (β, γ) values before and after the intervention.

The Fokker–Planck equation analysis provides a probabilistic view of Pg persistence, revealing that stochastic microenvironmental-sensing noise can sustain subcritical populations that would otherwise collapse deterministically. This noise is expected to be enhanced in *in vivo* settings, where microenvironmental complexity is much higher than in *in vitro* experiments. Quantitatively assessing the environmental noise requires special experiments such as intermittent fluid flow in the subgingival pocket that washes out quorum signaling, or temporal variance of Vp-derived heme measured via microfluidics. This observation bridges ecological modeling with the physics of decision-making in biological collectives. The bacterial population continuously samples its microenvironment, and random fluctuations in signaling effectively explore multiple "choices" between extinction and growth. Such stochastic switching mirrors cell-fate selection in multicellular systems, where intrinsic noise drives transitions between phenotypic attractors.

The cell decision-making aspect allows us to invoke the Least Microenvironmental Uncertainty Principle (LEUP) [52–56], where multicellular communities tend to minimize uncertainty about their microenvironment by adopting states that reduce phenotypic entropy. Within this framework, the switch between Pg extinction and Pg dominance can be viewed not only as a compositional phase transition but also as a collective decision-making process. Facilitation by Vp reduces environmental uncertainty, stabilizing a Pg-permissive niche. In contrast, interventions that enhance competition increase uncertainty for Pg and thereby promote extinction. This interpretation situates our results within a broader decision-theoretic framework that links microbial ecology with general principles of cellular adaptation.

Our study entails some limitations. First, the game-theoretic model is parameterized using Pg trajectories alone, which underdetermines the full payoff matrix. Direct co-culture experiments measuring both Pg and Vp abundances are needed to fully resolve the bacteria interactions. Second, we used a linear payoff structure, which cannot capture saturating metabolic interactions or context-dependent facilitation. In particular, the observed Pg decline after reaching the theoretical capacity indicates nutrient depletion, metabolic imbalance, or any other Pg stressor [31] production that could be modelled by additional non-linearities. Third, our stochastic analysis employed a Gaussian noise approximation and small-noise closure, which may not accurately represent bursty or correlated fluctuations *in vivo*. Finally, our model focuses on a two-species subsystem and ignores higher-order interactions with other oral taxa and host immune responses that could shift the location of the tipping point.

Future work should focus on quantifying the molecular basis of Vp facilitation, validating noise-induced persistence in controlled microfluidic systems, and calibrating

the game-theoretic model with high-resolution longitudinal multi-omics data. Integrating these approaches will enable predictive control of Pg-associated dysbiosis and inform the rational design of microbiome-targeted therapies aimed at restoring oral and systemic health [6, 7].

Methods

Experimental Basis

Our modeling is based on quantitative growth data, focusing on three key experimental series reported by Hoare et al. [15], as well as new experiments designed to validate the effects of stochasticity on Pg dynamics. As reported by Hoare et al. [15], single-species inoculum experiments were performed by culturing Pg strain 381 across a wide range of starting densities (10^5–10^8 cells/mL). Cultures were incubated anaerobically at 37 °C in mucin–serum medium (2.5 mg/mL hog gastric mucin, 2.0 mg/mL proteose peptone, 2.5 mg/mL KCl, 1.0 mg/mL trypticase peptone, 1.0 mg/mL yeast extract, 1.0 µg/mL cysteine HCl, 10% heat-inactivated human AB serum, 5 µg/mL hemin). Growth was monitored daily by qPCR targeting the 16S rRNA gene. These data were used to parameterize a cubic Allee-effect model capturing density-dependent deterministic dynamics. The resulting parameters then served as the baseline for our stochastic analysis of Pg population behavior, enabling us to examine how microenvironmental noise perturbs deterministic growth trajectories.

Second, we incorporated results from spent-medium complementation assays, in which cell-free supernatant from stationary-phase Vp cultures was added to low-density Pg inocula [15]. The spent medium of Vp was obtained by growing the bacteria in mucin–serum medium under anaerobic conditions for 24 hours. The cultures were then centrifuged, and the resulting supernatants were filter-sterilized twice using 0.22 µm filters to ensure removal of all cells. This sterile, cell-free spent medium was subsequently used at different proportions mixed with fresh medium, followed by inoculation of Pg at low-cell-density (10^5 cells/mL). While the experimental observations indicated rescue from extinction, model fitting allowed us to quantify the extent of threshold reduction through changes in the Allee parameter (A).

Third, Pg and Vp were co-inoculated into mucin–serum medium at a low cell density of 10^5 cells/mL each, and cultured under anaerobic conditions in a batch setup [15]. The cultures were incubated at 37 °C and sampled daily. The growth of Pg was quantitatively assessed using qPCR. This experimental design aimed to evaluate interspecies interactions between early colonizers like Vp and Pg. The observed growth of Pg from this co-culture experiment was used to inform and parameterize the explanatory two-species replicator model, which captures the frequency-dependent interactions and fitness landscape between the two species.

Fourth, to experimentally assess model predictions related to the influence of stochastic fluctuations, we conducted a new set of long-term monoculture experiments in which Pg was inoculated at a low cell density of 10^5 cells/mL in mucin–serum medium and monitored for up to 32 days (27 biological replicates). Cultures were sampled inside the anaerobic chamber, followed by serial dilutions and plating on Brain Heart Infusion agar supplemented with blood. Colony-forming units (CFUs)

were determined after 7 days of growth. These experiments also included co-cultures of Pg with Vp, with the latter either added at the beginning of the experiment as a co-culture control, or introduced after Pg had been incubated for 9 days to evaluate whether Pg populations could be rescued from extinction.

Computational Tools

All simulations and optimizations were conducted in Python 3.10. Core libraries included `NumPy` and `Pandas` for numerical operations, `SciPy` for integration and optimization, and `Matplotlib` for visualization. Custom implementations of the Euler-Maruyama scheme were used for stochastic integration.

Declarations

Data Availability

The datasets generated and/or analyzed during the current study are not publicly available due to institutional data management policies and the use of the data in ongoing longitudinal studies regarding oral microbiome transitions but are available from the corresponding author on reasonable request.

Code Availability

All computational analyses and modeling code supporting this study are publicly available on GitHub at: https://github.com/Moemenhussein11/P.gingivalis-Colonization

Acknowledgements

HH was supported by the RIG-2023-051 Khalifa University grant. PID acknowledges support from the National Institutes of Health, National Institute of Dental and Craniofacial Research (grant R21DE034093). HH, MQ, and PID acknowledge support from the UAE-NIH Collaborative Research grant AJF-NIH-25-KU. HH and AB acknowledge support from Volkswagenstiftung under the “Life?” program (grant 96732). MH acknowledges support from the Khalifa University PhD Program.

Author Contributions

Conceptualization: HH. Methodology: MH, AB, HH. Experiments: MS, PID. Investigation: MH, AB. Formal analysis: AB, MH. Writing — review and editing: MH, AB, MQ, MS, PID, HH. Supervision: HH. Funding acquisition: HH, MQ, PID.

Competing Interests

The authors declare no competing financial or non-financial interests.

References

[1] Sun, R., Zhou, Y., Pan, Q., Wang, R., Guo, Y., Huo, Y., Zhao, Y., Liu, M.: Changes and health inequalities in the global burden of periodontal diseases from 1990 to 2021: A population-based study. Clinical oral investigations **29**(10), 447 (2025) https://doi.org/10.1007/S00784-025-06558-0

[2] Fine, D.H., Schreiner, H.: Oral microbial interactions from an ecological perspective: a narrative review. Frontiers in oral health **4** (2023) https://doi.org/10.3389/FROH.2023.1229118

[3] Genco, R.J., Sanz, M.: Clinical and public health implications of periodontal and systemic diseases: An overview. Periodontology 2000 **83**(1), 7–13 (2020) https://doi.org/10.1111/prd.12344

[4] Hajishengallis, G.: Periodontitis: From microbial immune subversion to systemic inflammation. Nature Publishing Group (2015). https://doi.org/10.1038/nri3785

[5] Nadell, C.D., Drescher, K., Foster, K.R.: Spatial structure, cooperation and competition in biofilms. Nature reviews. Microbiology **14**(9), 589–600 (2016) https://doi.org/10.1038/NRMICRO.2016.84

[6] Baker, J.L., Mark Welch, J.L., Kauffman, K.M., McLean, J.S., He, X.: The oral microbiome: diversity, biogeography and human health. Nature reviews. Microbiology **22**(2), 89–104 (2024) https://doi.org/10.1038/S41579-023-00963-6

[7] Van Dyke, T.E., Bartold, P.M., Reynolds, E.C.: The Nexus Between Periodontal Inflammation and Dysbiosis. Frontiers in immunology **11** (2020) https://doi.org/10.3389/FIMMU.2020.00511

[8] Hooks, K.B., O'Malley, M.A.: Dysbiosis and its discontents. mBio **8**(5), 10–11280149217 (2017) https://doi.org/10.1128/mbio.01492-17 https://journals.asm.org/doi/pdf/10.1128/mbio.01492-17

[9] Hajishengallis, G., Lamont, R.J.: Polymicrobial communities in periodontal disease: their quasi-organismal nature and dialogue with the host. Periodontology 2000 **86**(1), 210 (2021) https://doi.org/10.1111/PRD.12371

[10] Hajishengallis, G., Liang, S., Payne, M.A., Hashim, A., Jotwani, R., Eskan, M.A., McIntosh, M.L., Alsam, A., Kirkwood, K.L., Lambris, J.D., Darveau, R.P., Curtis, M.A.: Low-abundance biofilm species orchestrates inflammatory periodontal disease through the commensal microbiota and complement. Cell host & microbe **10**(5), 497–506 (2011) https://doi.org/10.1016/J.CHOM.2011.10.006

[11] Hajishengallis, G., Chavakis, T.: Local and systemic mechanisms linking periodontal disease and inflammatory comorbidities. Nature Research (2021). https://doi.org/10.1038/s41577-020-00488-6

[12] Lamont, R.J., Kuboniwa, M.: The polymicrobial pathogenicity of Porphyromonas gingivalis. Frontiers in oral health **5** (2024) https://doi.org/10.3389/FROH.2024.1404917

[13] Fritts, R.K., McCully, A.L., McKinlay, J.B.: Extracellular Metabolism Sets the Table for Microbial Cross-Feeding. Microbiology and molecular biology reviews : MMBR **85**(1) (2021) https://doi.org/10.1128/MMBR.00135-20

[14] Morawska, L.P., Hernandez-Valdes, J.A., Kuipers, O.P.: Diversity of bet-hedging strategies in microbial communities-Recent cases and insights. WIREs mechanisms of disease **14**(2) (2022) https://doi.org/10.1002/WSBM.1544

[15] Hoare, A., Wang, H., Meethil, A., Abusleme, L., Hong, B.Y., Moutsopoulos, N.M., Marsh, P.D., Hajishengallis, G., Diaz, P.I.: A cross-species interaction with a symbiotic commensal enables cell-density-dependent growth and in vivo virulence of an oral pathogen. ISME Journal **15**(5), 1490–1504 (2021) https://doi.org/10.1038/s41396-020-00865-y

[16] Muir, E.J., Lajeunesse, M.J., Kramer, A.M.: The magnitude of Allee effects varies across Allee mechanisms, but not taxonomic groups. Oikos **2024**(7), 10386 (2024) https://doi.org/10.1111/OIK.10386

[17] Lamell, C.W., Griffen, A.L., McClellan, D.L., Leys, E.J.: Acquisition and Colonization Stability of Actinobacillus actinomycetemcomitans and Porphyromonas gingivalis in Children. Journal of Clinical Microbiology **38**(3), 1196 (2000) https://doi.org/10.1128/JCM.38.3.1196-1199.2000

[18] Griffen, A.L., Becker, M.R., Lyons, S.R., Moeschberger, M.L., Leys, E.J.: Prevalence of Porphyromonas gingivalis and Periodontal Health Status. Journal of Clinical Microbiology **36**(11), 3239 (1998) https://doi.org/10.1128/JCM.36.11.3239-3242.1998

[19] Ehmke, B., Moter, A., Beikler, T., Milian, E., Flemmig, T.F.: Adjunctive antimicrobial therapy of periodontitis: long-term effects on disease progression and oral colonization. Journal of periodontology **76**(5), 749–759 (2005) https://doi.org/10.1902/JOP.2005.76.5.749

[20] Fujise, O., Miura, M., Hamachi, T., Maeda, K.: Risk of Porphyromonas gingivalis recolonization during the early period of periodontal maintenance in initially severe periodontitis sites. Journal of periodontology **77**(8), 1333–1339 (2006) https://doi.org/10.1902/JOP.2006.050225

[21] Mombelli, A.: Microbial colonization of the periodontal pocket and its significance for periodontal therapy. Periodontology 2000 **76**(1), 85–96 (2018) https://doi.org/10.1111/PRD.12147

[22] Markowska, K., Szymanek-Majchrzak, K., Pituch, H., Majewska, A.: Understanding Quorum-Sensing and Biofilm Forming in Anaerobic Bacterial Communities. International journal of molecular sciences **25**(23) (2024) https://doi.org/10.3390/IJMS252312808

[23] Zhou, P., Manoil, D., Belibasakis, G.N., Kotsakis, G.A.: Veillonellae: Beyond Bridging Species in Oral Biofilm Ecology. Frontiers in oral health **2** (2021) https://doi.org/10.3389/FROH.2021.774115

[24] Periasamy, S., Kolenbrander, P.E.: Central role of the early colonizer Veillonella sp. in establishing multispecies biofilm communities with initial, middle, and late colonizers of enamel. Journal of bacteriology **192**(12), 2965–2972 (2010) https://doi.org/10.1128/JB.01631-09

[25] Periasamy, S., Kolenbrander, P.E.: Mutualistic Biofilm Communities Develop with Porphyromonas gingivalis and Initial, Early, and Late Colonizers of Enamel. Journal of Bacteriology **191**(22), 6804 (2009) https://doi.org/10.1128/JB.01006-09

[26] Urbaniec, J., Xu, Y., Hu, Y., Hingley-Wilson, S., McFadden, J.: Phenotypic heterogeneity in persisters: a novel 'hunker' theory of persistence. FEMS Microbiology Reviews **46**(1), 042 (2021) https://doi.org/10.1093/FEMSRE/FUAB042

[27] Allen, B., Nowak, M.A.: Cooperation and the Fate of Microbial Societies. PLoS Biology **11**(4), 1001549 (2013) https://doi.org/10.1371/JOURNAL.PBIO.1001549

[28] Zomorrodi, A.R., Segrè, D.: Genome-driven evolutionary game theory helps understand the rise of metabolic interdependencies in microbial communities. Nature communications **8**(1) (2017) https://doi.org/10.1038/S41467-017-01407-5

[29] Sun, G.Q.: Mathematical modeling of population dynamics with Allee effect. Springer (2016). https://doi.org/10.1007/s11071-016-2671-y

[30] Storn, R., Price, K.: Differential Evolution - A Simple and Efficient Heuristic for Global Optimization over Continuous Spaces. Journal of Global Optimization **11**(4), 341–359 (1997) https://doi.org/10.1023/A:1008202821328/METRICS

[31] Lamont, R.J., Jenkinson, H.F.: Life below the gum line: pathogenic mechanisms of Porphyromonas gingivalis. Microbiology and molecular biology reviews : MMBR **62**(4), 1244–1263 (1998) https://doi.org/10.1128/MMBR.62.4.1244-1263.1998

[32] Mukherjee, S., Bassler, B.L.: Bacterial quorum sensing in complex and dynamically changing environments. Nature Reviews Microbiology **17**(6), 371–382 (2019) https://doi.org/10.1038/s41579-019-0186-5

[33] Hoek, T.A., Axelrod, K., Biancalani, T., Yurtsev, E.A., Liu, J., Gore, J.: Resource Availability Modulates the Cooperative and Competitive Nature of a Microbial Cross-Feeding Mutualism. PLoS Biology **14**(8), 1–17 (2016) https://doi.org/10.1371/journal.pbio.1002540

[34] García-Ojalvo, J., Sancho, J.M.: Noise in Spatially Extended Systems. Institute for Nonlinear Science, pp. 1–22. Springer, New York, NY (1999). https://doi.org/10.1007/978-1-4612-1536-3 . http://link.springer.com/10.1007/978-1-4612-1536-3

[35] Méndez, V., Llopis, I., Campos, D., Horsthemke, W.: Effect of environmental fluctuations on invasion fronts. Journal of Theoretical Biology **281**(1), 31–38 (2011) https://doi.org/10.1016/j.jtbi.2011.04.025

[36] Naito, M., Hirakawa, H., Yamashita, A., Ohara, N., Shoji, M., Yukitake, H., Nakeyama, K., Toh, H., Yoshimura, F., Kuhara, S., Hattori, M., Hayashi, T., Nakayama, K.: Determination of the genome sequence of Porphyromonas glnglvalls strain ATCC 33277 and genomic comparison with strain W83 revealed extensive genome rearrangements in P. glnglvalls. DNA Research **15**(4), 215–225 (2008) https://doi.org/10.1093/dnares/dsn013

[37] Reichert-Schwillinsky, F., Pin, C., Dzieciol, M., Wagner, M., Hein, I.: Stress- and growth rate-related differences between plate count and real-time PCR data during growth of Listeria monocytogenes. Applied and Environmental Microbiology **75**(7), 2132–2138 (2009) https://doi.org/10.1128/AEM.01796-08

[38] Taylor, P.D., Jonker, L.B.: Evolutionarily stable strategies with two types of players. Mathematical Biosciences **40**(1-2), 145–156 (1978) https://doi.org/10.1016/0025-5564(78)90077-9

[39] Cressman, R.: Replicator dynamics. Encyclopedia of Complexity and Systems Science, 5546–5561 (2009)

[40] Abdulkareem, A.A., Al-Taweel, F.B., Al-Sharqi, A.J.B., Gul, S.S., Sha, A., Chapple, I.L.C.: Current concepts in the pathogenesis of periodontitis: from symbiosis to dysbiosis. Journal of oral microbiology **15**(1) (2023) https://doi.org/10.1080/20002297.2023.2197779

[41] Abisado, R.G., Benomar, S., Klaus, J.R., Dandekar, A.A., Chandler, J.R.: Bacterial Quorum Sensing and Microbial Community Interactions. mBio **9**(3) (2018) https://doi.org/10.1128/MBIO.02331-17

[42] Ammann, T.W., Belibasakis, G.N., Thurnheer, T.: Impact of early colonizers on in vitro subgingival biofilm formation. PloS one **8**(12) (2013) https://doi.org/10.1371/JOURNAL.PONE.0083090

[43] Dennis, B.: Allee effects in stochastic populations. Oikos **96**(3), 389–401 (2002) https://doi.org/10.1034/j.1600-0706.2002.960301.x

[44] Dennis, B., Assas, L., Elaydi, S., Kwessi, E., Livadiotis, G.: Allee effects and resilience in stochastic populations. Theoretical Ecology **9**(3), 323–335 (2016) https://doi.org/10.1007/S12080-015-0288-2/FIGURES/7

[45] Gong, A., Walker, E.J., Gilbert, B.: Allee Effects, Colonization, and Extinction: The Surprising Benefits of Demographic Stochasticity. The American naturalist **206**(1), 31–43 (2025) https://doi.org/10.1086/735833

[46] Balaban, N.Q., Merrin, J., Chait, R., Kowalik, L., Leibler, S.: Bacterial persistence as a phenotypic switch. Science (New York, N.Y.) **305**(5690), 1622–1625 (2004) https://doi.org/10.1126/SCIENCE.1099390

[47] Madianos, P.N., Papapanou, P.N., Nannmark, U., Dahlén, G., Sandros, J.: Porphyromonas gingivalis FDC381 multiplies and persists within human oral epithelial cells in vitro. Infection and immunity **64**(2), 660–664 (1996) https://doi.org/10.1128/IAI.64.2.660-664.1996

[48] Leea, K., Robertsb, J.A.S., Choic, C.H., Atanasova, K.R., Yilmaz, O.: Porphyromonas gingivalis traffics into endoplasmic reticulum-rich-autophagosomes for successful survival in human gingival epithelial cells. Virulence **9**(1), 845 (2018) https://doi.org/10.1080/21505594.2018.1454171

[49] Li, P., Fung, Y.M.E., Yin, X., Seneviratne, C.J., Che, C.M., Jin, L.: Controlled cellular redox, repressive hemin utilization and adaptive stress responses are crucial to metronidazole tolerance of Porphyromonas gingivalis persisters. Journal of clinical periodontology **45**(10), 1211–1221 (2018) https://doi.org/10.1111/JCPE.13002

[50] Wang, C., Li, X., Cheng, T., Sun, H., Jin, L.: Eradication of Porphyromonas gingivalis Persisters Through Colloidal Bismuth Subcitrate Synergistically Combined With Metronidazole. Frontiers in microbiology **12** (2021) https://doi.org/10.3389/FMICB.2021.748121

[51] Wang, C., Cheng, T., Li, X., Jin, L.: Metronidazole-Treated Porphyromonas gingivalis Persisters Invade Human Gingival Epithelial Cells and Perturb Innate Responses. Antimicrobial agents and chemotherapy **64**(6) (2020) https://doi.org/10.1128/AAC.02529-19

[52] Hatzikirou, H.: Statistical mechanics of cell decision-making: the cell migration force distribution. Journal of the Mechanical Behavior of Materials **27**(1-2), 20180001 (2018) https://doi.org/10.1515/jmbm-2018-0001

[53] Barua, A., Nava-Sedeño, J.M., Meyer-Hermann, M., Hatzikirou, H.: A least microenvironmental uncertainty principle (leup) as a generative model of collective cell migration mechanisms. Sci. Rep. **10**, 22371 (2020) https://doi.org/10.1038/s41598-020-79119-y

[54] Barua, A., Syga, S., Mascheroni, P., Kavallaris, N., Meyer-Hermann, M., Deutsch, A., Hatzikirou, H.: Entropy-driven cell decision-making predicts 'fluid-to-solid' transition in multicellular systems. New J. Phys. **22**, 123034 (2020) https://doi.org/10.1088/1367-2630/abcb2e

[55] Pujar, A.A., Barua, A., Dey, P.S., Singh, D., Roy, U., Jolly, M.K., Hatzikirou, H.: Microenvironmental entropy dynamics analysis reveals novel insights into Notch-Delta-Jagged decision-making mechanism. iScience **27**(9), 110569 (2024) https://doi.org/10.1016/j.isci.2024.110569

[56] Barua, A., Hatzikirou, H.: Cell Decision Making through the Lens of Bayesian Learning. Entropy **25**(4), 609 (2023) https://doi.org/10.3390/e25040609 arXiv:2301.06941

Tables

Table 1: Biological interpretation of the replicator dynamics across the (β, γ) plane for $x \in [0, 1]$ (cf. Figure 6).

Region	**Condition**	**Attractors**[a]
Pg extinction	$\beta < 0,\ \beta + \gamma < 0,$	$x = 0$ stable
Pg dominance	$\beta > 0,\ \beta + \gamma > 0,$	$x = 1$ stable
Coexistence	$\beta > 0,\ \beta + \gamma < 0$	$x = 0$ and $x = 1$ unstable; $x^\star$ stable
Bistable	$\beta < 0,\ \beta + \gamma > 0$	$x = 0$ and $x = 1$ stable; $x^\star$ unstable

[a] $x^\star$ denotes the interior fixed point (when it exists).

Figure Legends

Figure 1. Model fitting results across four initial inoculum sizes. Scatter points represent observed values of $\log_{10}(N)$ over time, while solid lines show predictions from the fitted model. Each color/marker denotes a distinct initial 10^x inoculum level.

Figure 2. Effect of Vp-derived spent medium on Pg population growth and fitted parameters. (a) Model predictions versus experimental observations across different Vp spent-medium (SM) percentages. Scatter points represent observed values of $\log_{10}(N)$ over time, while solid lines show predictions from the fitted model using mean parameter estimates. Each color/marker corresponds to a distinct condition (% Vp SM). (b) Variation of fitted model parameters with Vp SM percentage. Estimated parameter values are shown as mean ± SEM for intrinsic growth rate r, carrying capacity K, and critical mass A. Dashed horizontal lines indicate the reference mean parameter values obtained from simulations without Vp SM ($K = 2.08 \times 10^9$, $A = 4.59 \times 10^7$, and $r = 0.6529$).

Figure 3. Illustrative nullcline plot of the bacterial population under two noise strengths. Parameters ($K = 100$, $A = 25$, $r_m = 1$) were chosen to demonstrate the qualitative effect of noise on the Allee threshold.

Figure 4. Stochastic simulations of bacterial population dynamics under different perturbation strengths. (a) Bacterial population dynamics trajectories initiated above the Allee threshold (10^8 cells). Each curve represents the mean across 100 independent stochastic trajectories, with shaded regions denoting the standard error of the mean. Model parameters were obtained by fitting an Allee-effect growth model to experimental growth curves ($K = 2.08 \times 10^9$, $A = 4.59 \times 10^7$, and $r = 0.6529$). (b) Bacterial population dynamics trajectories initiated below the Allee threshold (10^5 cells). Each curve represents the mean across 100 independent stochastic trajectories, with shaded regions denoting the standard error of the mean. Model parameters were obtained by fitting an Allee-effect growth model to experimental growth curves ($K = 2.08 \times 10^9$, $A = 4.59 \times 10^7$, and $r = 0.6529$).

Figure 5. Experimental validation of the stochastic persistence model for Pg subthreshold populations. (a) Temporal trajectories of Pg populations initiated below the Allee threshold (10^5 cells). Each line represents a biological replicate, color-coded to reflect distinct dynamical behaviors. (b) Distribution and power-law fit of the steady-state Pg population size N. The histogram shows the frequency of population sizes, while circles represent the empirical density $P(N)$. The x-axis is shown on a logarithmic scale. A green line over the fitted regime indicates a power-law fit applied to the lower-bound population density.

Figure 6. Phase-space plot of Pg–Vp interactions. The line $\beta + \gamma = 0$ is shown as a dotted line and $\beta = 0$ is shown as a solid line.

Figure 7. Pg–Vp co-culture experiments and interaction phase space. (a) Vp rescues Pg from extinction. Each line represents an individual replicate time-course of Pg abundance. Lines sharing the same color denote replicates exhibiting similar outcomes. Early Vp introduction promotes sustained Pg growth, whereas delayed introduction leads to divergent outcomes. (b) Experimentally constrained interaction phase space indicating the inferred form of bacterial interactions. Created in BioRender. Hussein, M. (2026) https://BioRender.com/vvmikxi.

Figure 8. Overview of ecological processes influencing Pg persistence. In the deterministic framework, population survival depends on a minimum density, below which extinction occurs and above which growth is maintained. Early colonizing species, such as Vp, provide metabolic support that allows Pg to establish even when present at low abundance. Random fluctuations in the environment, as well as intrinsic differences among individual cells, create variability that increases the likelihood of survival under adverse conditions. Created in BioRender. Hussein, M. (2026) https://BioRender.com/quam553.

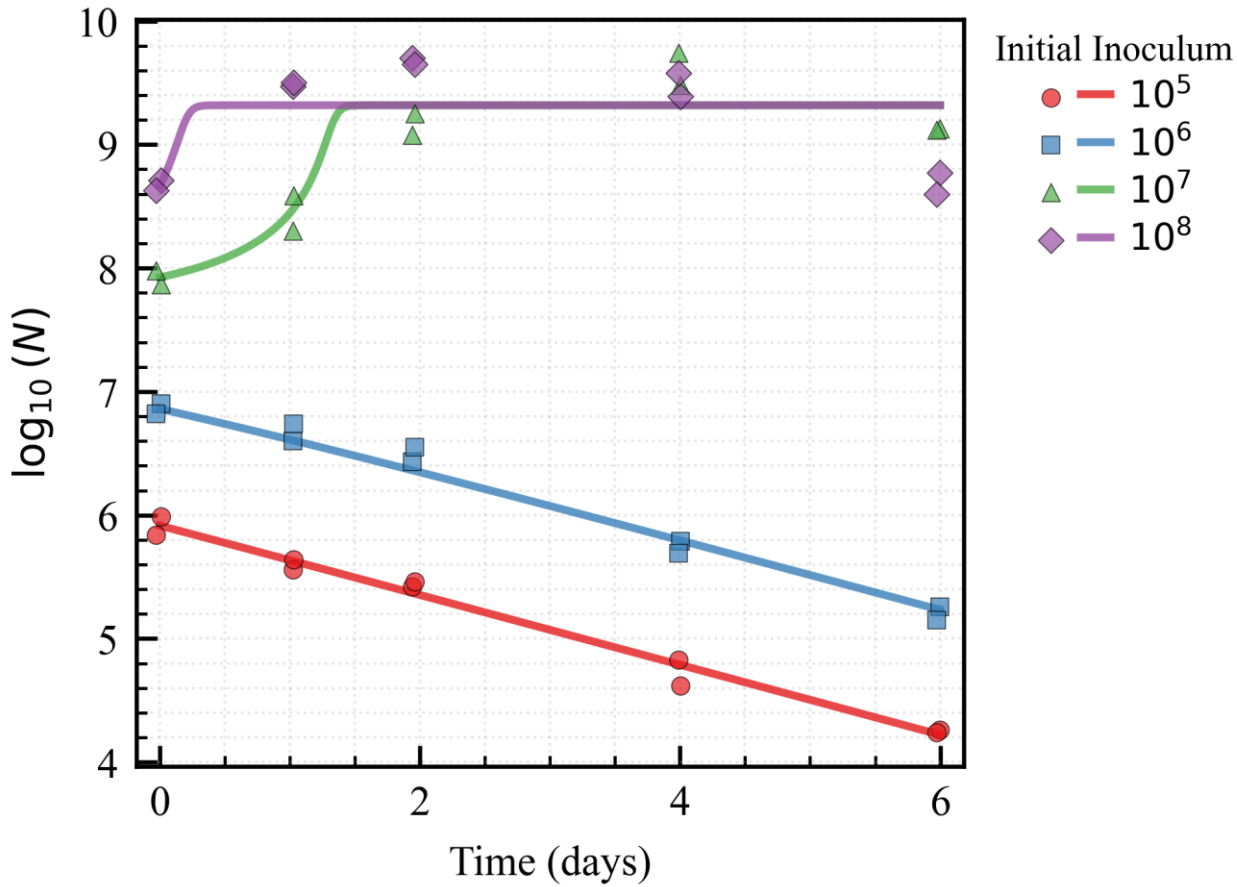
10
9
8
7
6
5
4
log10 (N)
0
2
4
6
Time (days)
Initial Inoculum
10^5
10^6
10^7
10^8

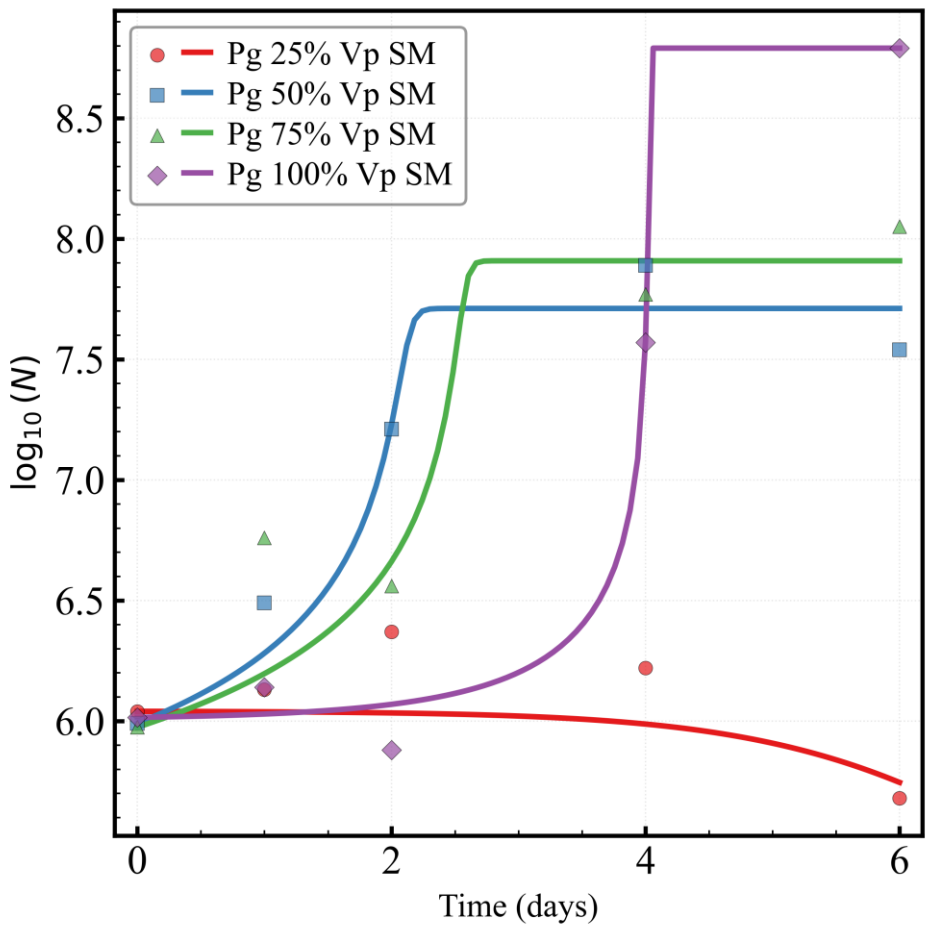
Pg 25% Vp SM
Pg 50% Vp SM
Pg 75% Vp SM
Pg 100% Vp SM
log10 (N)
8.5
8.0
7.5
7.0
6.5
6.0
0
2
4
6
Time (days)

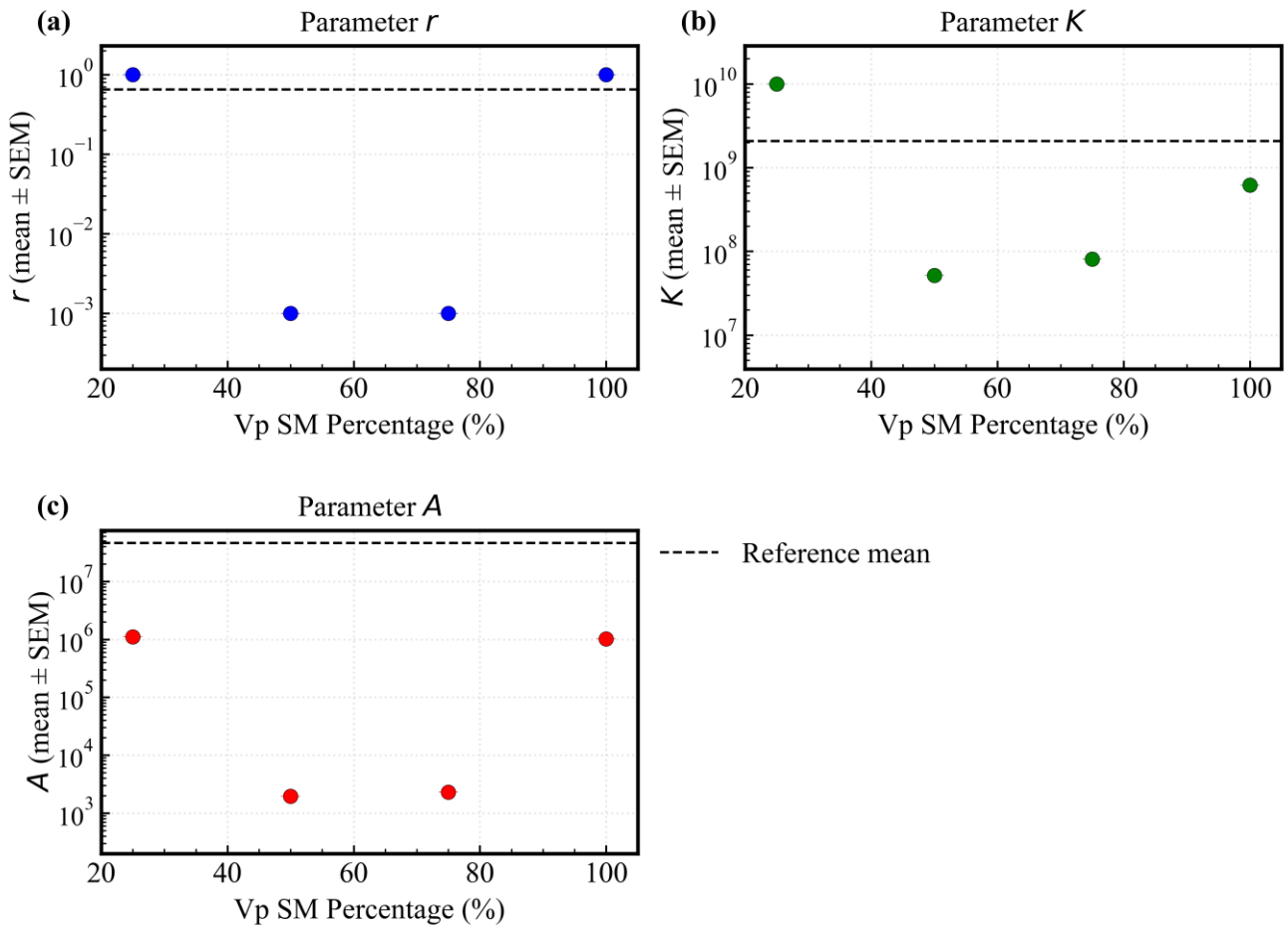
(a)
Parameter r
r (mean ± SEM)
Vp SM Percentage (%)
(b)
Parameter K
K (mean ± SEM)
Vp SM Percentage (%)
(c)
Parameter A
A (mean ± SEM)
Vp SM Percentage (%)
Reference mean

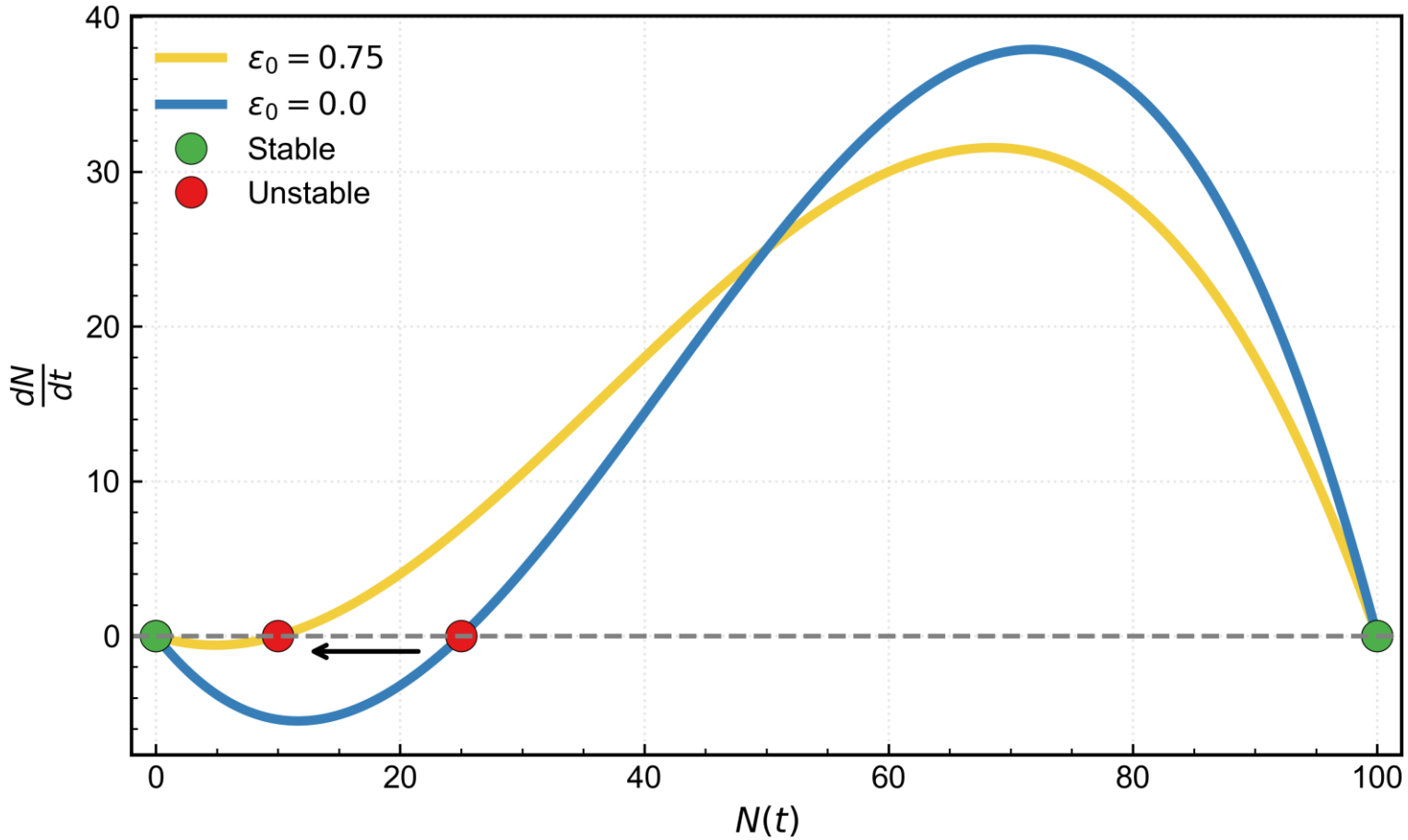
$\varepsilon_0 = 0.75$
$\varepsilon_0 = 0.0$
Stable
Unstable
$\frac{dN}{dt}$
$N(t)$
40
30
20
10
0
0
20
40
60
80
100

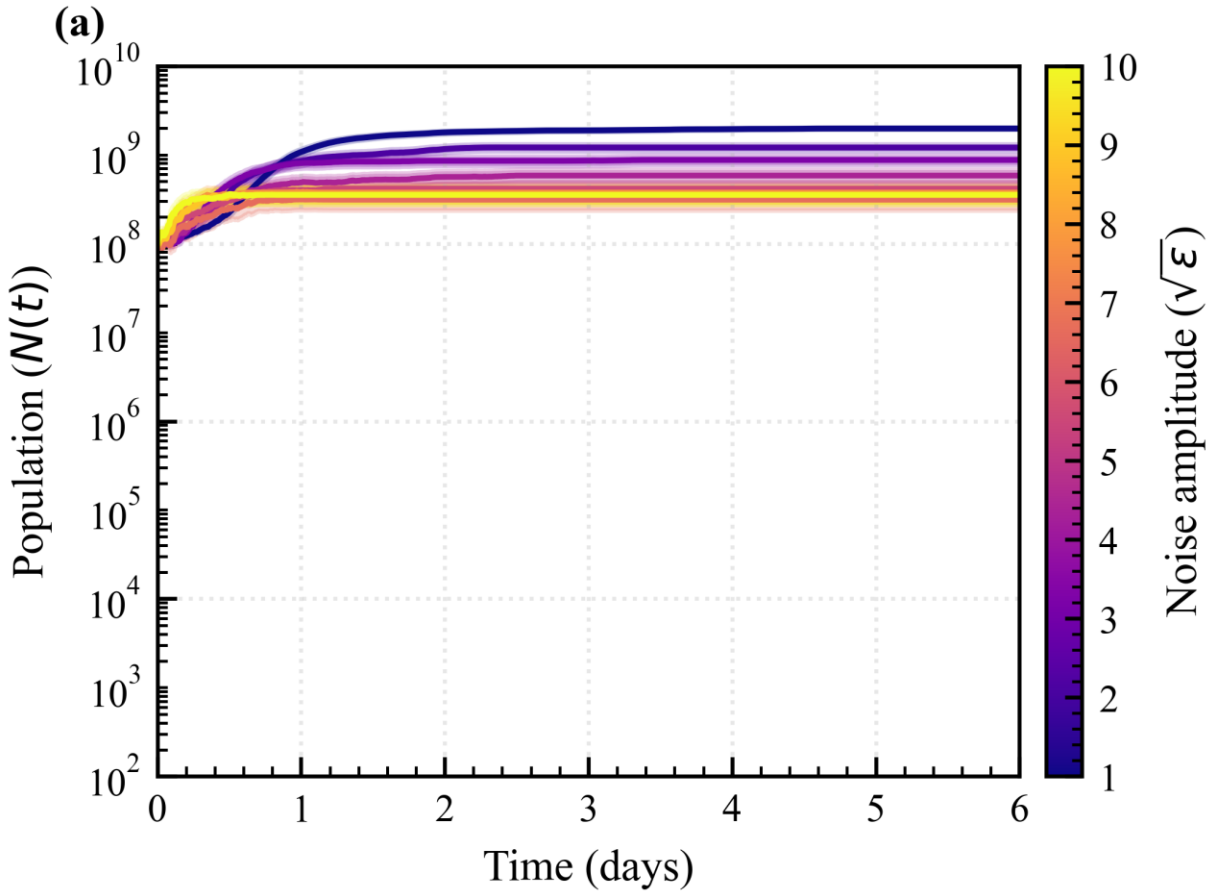
(a)
Population ($N(t)$)
10^{10}
10^{9}
10^{8}
10^{7}
10^{6}
10^{5}
10^{4}
10^{3}
10^{2}
0
1
2
3
4
5
6
Time (days)
10
9
8
7
6
5
4
3
2
1
Noise amplitude ($\sqrt{\varepsilon}$)

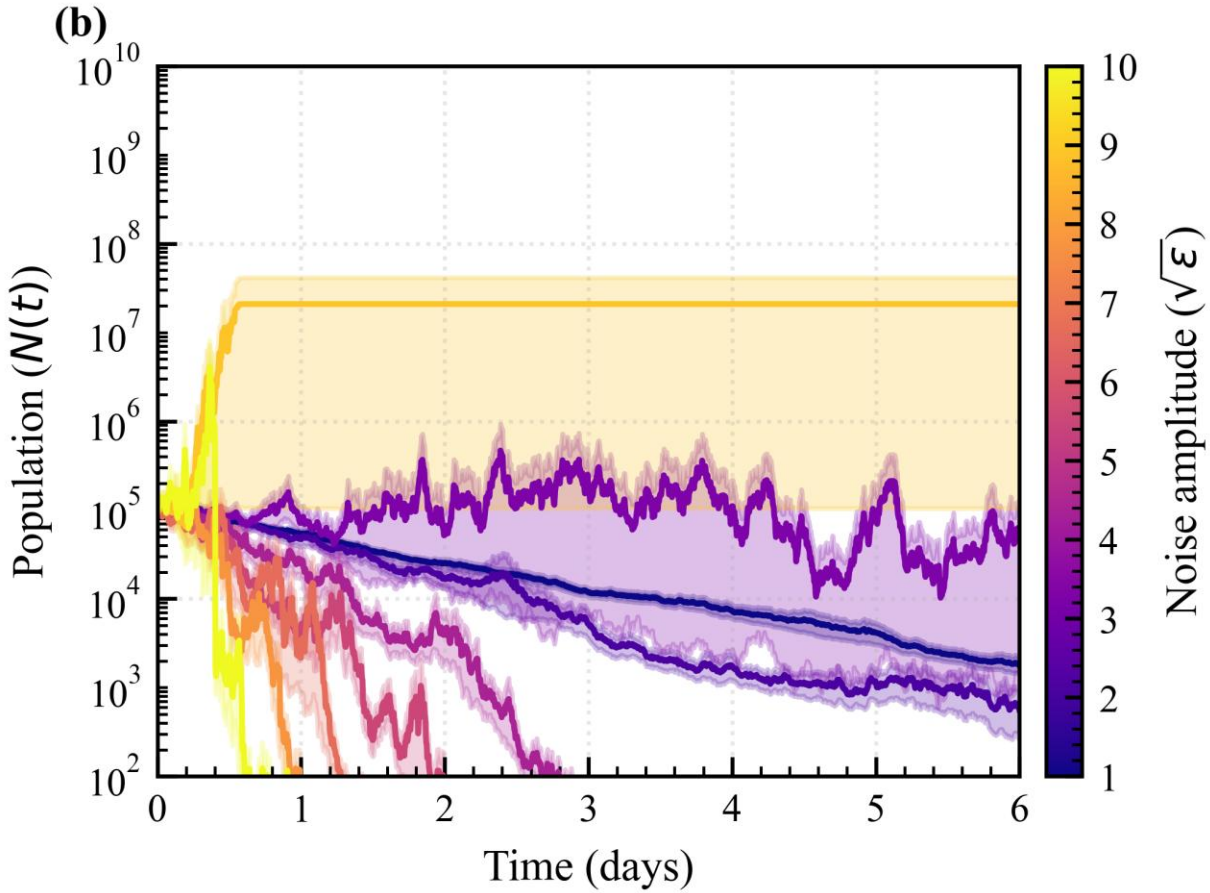
(b)
Population ($N(t)$)
10^{10}
10^{9}
10^{8}
10^{7}
10^{6}
10^{5}
10^{4}
10^{3}
10^{2}
0
1
2
3
4
5
6
Time (days)
10
9
8
7
6
5
4
3
2
1
Noise amplitude ($\sqrt{\varepsilon}$)

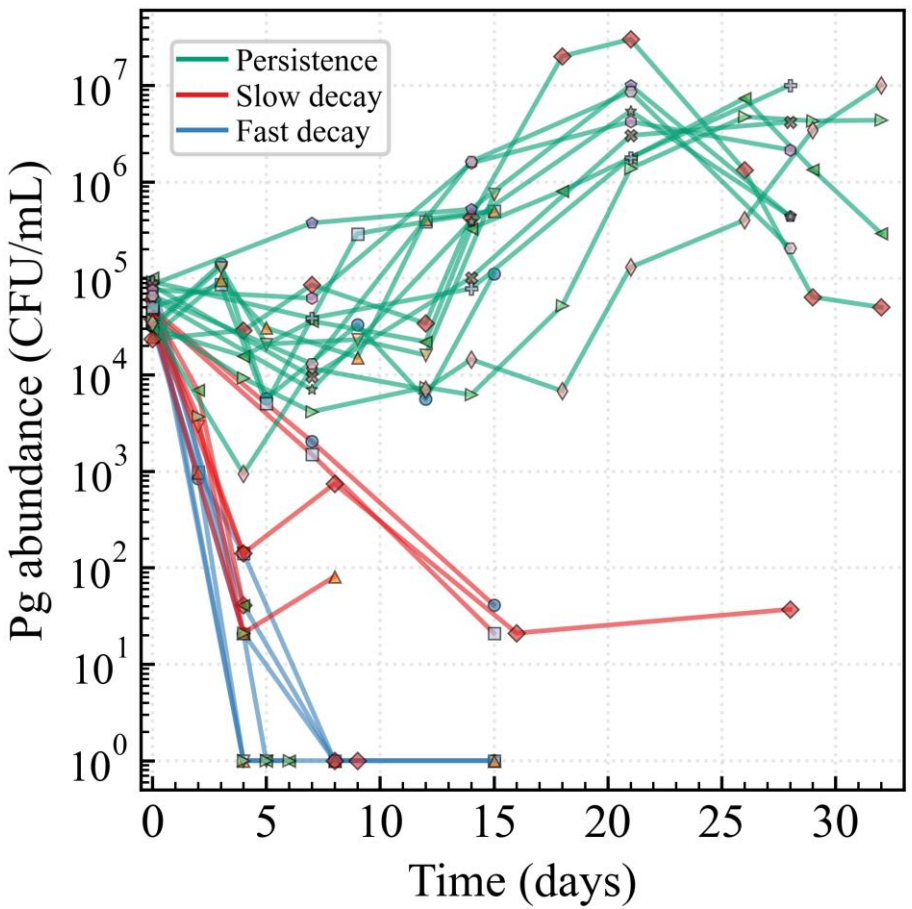
Persistence
Slow decay
Fast decay
Pg abundance (CFU/mL)
10^0
10^1
10^2
10^3
10^4
10^5
10^6
10^7
0
5
10
15
20
25
30
Time (days)

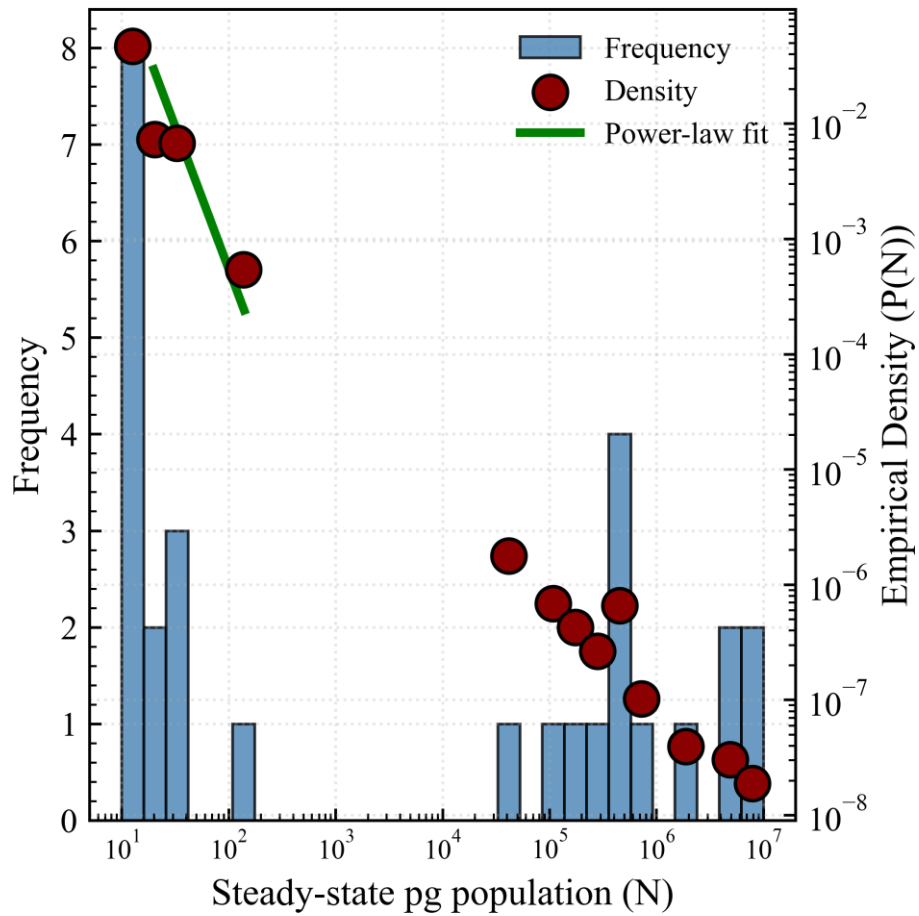
Frequency
Density
Power-law fit
Frequency
Empirical Density (P(N))
Steady-state pg population (N)
0
1
2
3
4
5
6
7
8
10^{-2}
10^{-3}
10^{-4}
10^{-5}
10^{-6}
10^{-7}
10^{-8}
10^{1}
10^{2}
10^{3}
10^{4}
10^{5}
10^{6}
10^{7}

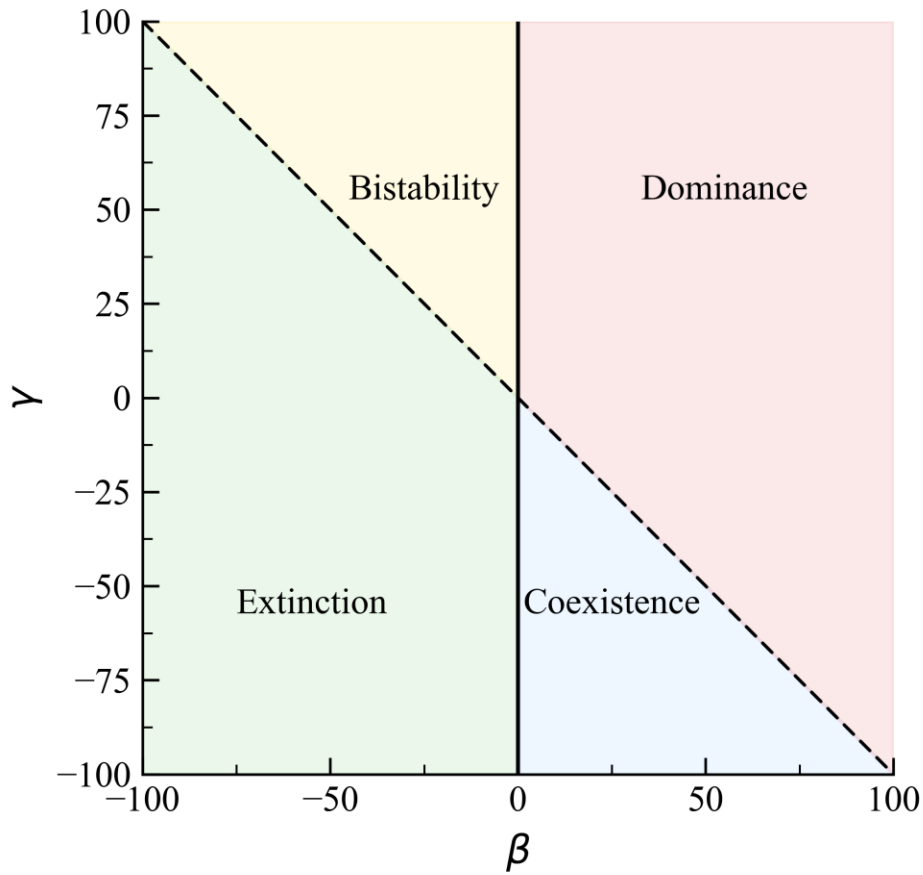
100
75
50
25
0
−25
−50
−75
−100
−100
−50
0
50
100
γ
β
Bistability
Dominance
Extinction
Coexistence

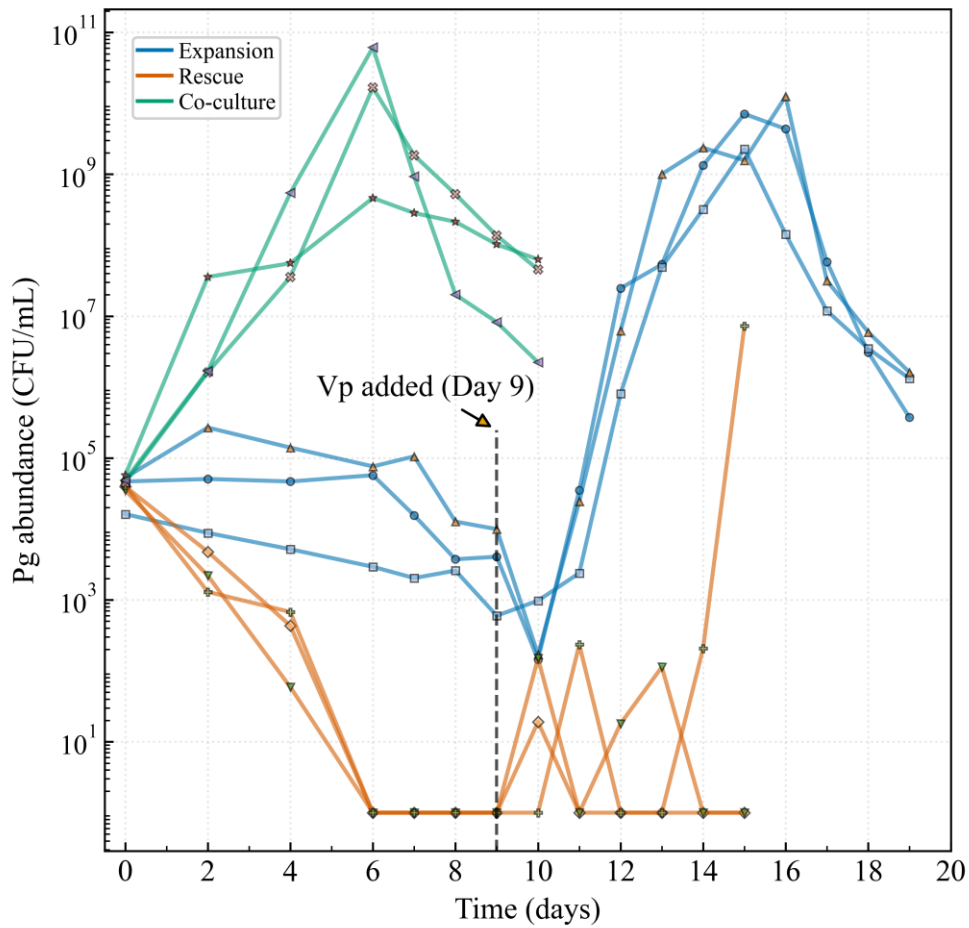
Expansion
Rescue
Co-culture
Vp added (Day 9)
Pg abundance (CFU/mL)
Time (days)
10^{11}
10^{9}
10^{7}
10^{5}
10^{3}
10^{1}
0
2
4
6
8
10
12
14
16
18
20

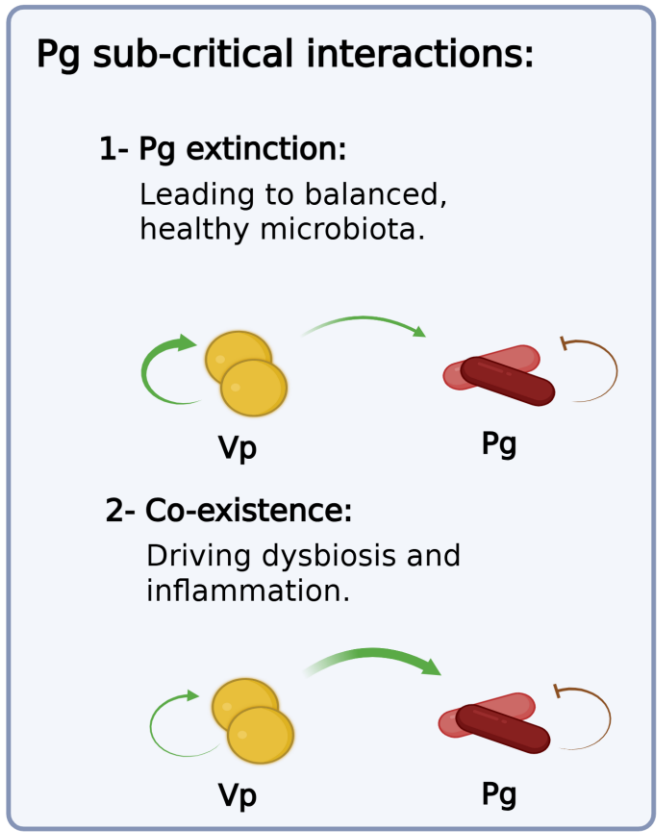
Pg sub-critical interactions:
1- Pg extinction:
Leading to balanced, healthy microbiota.
Vp
Pg
2- Co-existence:
Driving dysbiosis and inflammation.
Vp
Pg

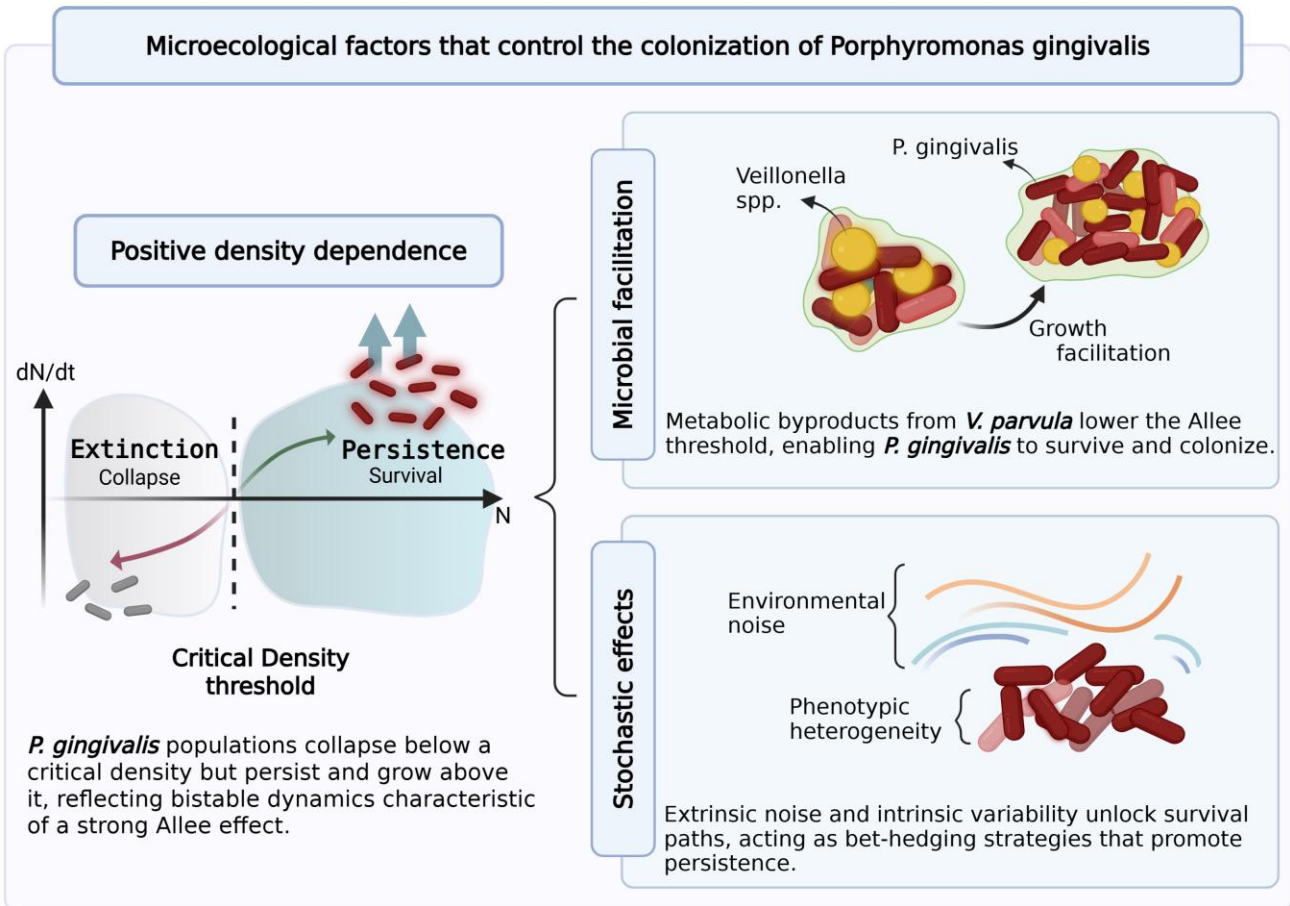
Microecological factors that control the colonization of Porphyromonas gingivalis
Positive density dependence
dN/dt
Extinction
Collapse
Persistence
Survival
N
Critical Density threshold
P. gingivalis populations collapse below a critical density but persist and grow above it, reflecting bistable dynamics characteristic of a strong Allee effect.
Microbial facilitation
P. gingivalis
Veillonella spp.
Growth facilitation
Metabolic byproducts from V. parvula lower the Allee threshold, enabling P. gingivalis to survive and colonize.
Stochastic effects
Environmental noise
Phenotypic heterogeneity
Extrinsic noise and intrinsic variability unlock survival paths, acting as bet-hedging strategies that promote persistence.